Aliphatic polycarbonate-based polyurethane elastomers and nanocomposites. I. The influence of hard-segment content and macrodiol-constitution on bottom-up self-assembly

ARTICLE *in* JOURNAL OF APPLIED POLYMER SCIENCE · NOVEMBER 2012

Impact Factor: 1.77 · DOI: 10.1002/app.36993

6 AUTHORS, INCLUDING:

Milena Špírková
Academy of Sciences of the Czech Republic
145 PUBLICATIONS **1,432** CITATIONS
SEE PROFILE

Rafał Poręba
Academy of Sciences of the Czech Republic
17 PUBLICATIONS **140** CITATIONS
SEE PROFILE

J. Pavličević
University of Novi Sad
44 PUBLICATIONS **184** CITATIONS
SEE PROFILE

Libor Kobera
University of Ottawa
30 PUBLICATIONS **127** CITATIONS
SEE PROFILE

Aliphatic Polycarbonate-Based Polyurethane Elastomers and Nanocomposites. I. The Influence of Hard-Segment Content and Macrodiol-Constitution on Bottom-Up Self-Assembly

Milena Špírková,[1] Rafał Poręba,[1] Jelena Pavličević,[1]* Libor Kobera,[2] Josef Baldrian,[2] Michal Pekárek[2]

[1]*Nanostructured Polymers and Composites Department, Institute of Macromolecular Chemistry, Academy of Sciences of the Czech Republic, 162 06 Prague 6, Czech Republic*
[2]*Institute of Macromolecular Chemistry, Academy of Sciences of the Czech Republic, 162 06 Prague 6, Czech Republic*

Received 27 October 2011; accepted 12 February 2012
DOI 10.1002/app.36993
Published online 16 April 2012 in Wiley Online Library (wileyonlinelibrary.com).

ABSTRACT: Aliphatic polycarbonate-based polyurethane (PC-PU) elastomers as well as their nanocomposites with organic-modified clay (bentonite for organic system) were synthesized. Macrodiols (MD) (randomly copolymerized aliphatic PC-glycols of molecular weight of about 2000: T5652, T4672, and T4692), hexamethylene diisocyanate, and butane-1,4-diol were used as starting materials. Solid-state NMR and Fourier transform infrared spectroscopy, small-angle X-ray scattering, wide-angle X-ray diffraction, atomic force microscopy, and transmission electron microscopy were used for studying the bottom-up self-assembly of building units from the segmental level up that of organized structures of micrometer sizes. Contents of hard segments formed by the reaction of chain extender with diisocyanate plays a dominant role for the degree of ordering and related phenomena, while the MD chain has only limited effect on PC-PU properties. The spectroscopy and scattering experiments suggest that bentonite particles incorporate well in the structure and promote the ordering of hard segment domains in PC-PU matrix as compared with the nanofiller-free analogue. © 2012 Wiley Periodicals, Inc. J Appl Polym Sci 126: 1016–1030, 2012

Key words: polyurethane elastomer; polycarbonate diol; nanocomposite; hydrogen bonding; self-assembly

INTRODUCTION

Polyurethanes (PUs) prepared from macrodiol (MD), diisocyanate, and chain extender ("short" diol) belong to typical thermoplastic elastomers. The thermoplastic polyurethanes (TPU) are mostly linear multiblock copolymers containing soft segments formed by MD and hard segments (HS) which are reaction products of chain extender with diisocyanate. The incompatibility of hard and soft segments leads to microphase-segregated structure of TPUs, which is very important for their properties.[1,2] Soft segments in conventional PU elastomers are built from either polyether or polyester MDs. Numerous studies using wide varieties of experimental techniques were used to understand the structure–property relationship using this kind of MDs.[1–6] However, TPUs based on recently quite popular poly(alkylene) carbonate (PC) MDs are more and more used in current PU formulations.[7–13] While the soft segments (not depending on the nature of MDs) provide elastomeric features of the TPUs, the HS serve as the material reinforcement, because they assure physical crosslinking of the system by hydrogen bonds, the impact of which is fairly similar to that based on chemical bonds in rubber materials. TPU elastomers thus exhibit the rubber-like behavior; however (unlike conventional rubbers) they can be processed and recycled like thermoplastics. Even though the interest of scientists and manufacturers in TPUs covers the period of almost 70 years, TPU, their nanocomposites, and blends are still attractive not only for industrial and practical applications, but also from the academic point of view.[3,5,11,14–18]

As mentioned, polycarbonate-based polyurethane (PC-PU) elastomers belong to a relatively new and

**Present address:* Faculty of Technology, Department of Materials Engineering, University of Novi Sad, Bul. Cara Lazara 1, 21000 Novi Sad, Serbia.
Correspondence to: M. Špírková (spirkova@imc.cas.cz).
Contract grant sponsor: Grant Agency of the Czech Republic (Czech Science Foundation); contract grant number: P108/10/0195.
Contract grant sponsor: Serbian Ministry of Education and Science; contract grant number: 45022.

promising group of TPUs.[7–13,19–26] Aromatic di- and polyisocyanates based on 4,4′-diphenylmethane diisocyanate are the mostly used in TPUs,[3,4,7–12,14–17,19,21,26] but aliphatic, mainly hexamethylene diisocyanate (HDI),[5,6,13,15,18,20,22–25] started to be more and more popular in current polyurethane formulations. The main disadvantage of PC-PUs as compared with "classical" polyether- or polyester-based PUs is their high cost, but their superior mechanical, biological, heat-, oxidative-, hydrolysis- and UV-light resistant properties[8,9,21,25,27] usually compensate the cost drawback.

Thanks to a number of modern medical applications,[10,12,18,20,21,27] many formulations of PC-based PUs have been patented. However, the application potential of PU materials is far from being exploited and therefore detailed studies of the structure–properties relationship of well-defined materials (including details of their preparation) are needed. Only when all details of the bottom-up development of functional properties (starting at the segmental level) are revealed, new targeted materials with desired end-use properties can be developed and manufactured.

PC diols are prepared mostly by the reaction of alkane diol with dialkylcarbonates. The most popular aliphatic polycarbonate diols (PCD) are based on poly(hexamethylene carbonate) diol,[7,9,11,12,21,25,26] or on PCD copolymers containing 2–10 alkane units.[8,10,13,22–25] From a number of relevant papers on PC-PUs, it is obvious that mechanical, thermal, and morphological properties of PC-PUs are affected mainly by chemical structure and molecular weight of PC diols.[7–13,19–27] PUs based on polycarbonates predominantly exhibit high tensile strength and modulus, but their elasticity is sometimes lower due to the high degree of phase mixing created by hydrogen bonding between soft segment carbonate and hard segment urethane groups. Only a proper balance of the phase mixing and phase separation can provide materials with low modulus, high elasticity, high tensile strength, and toughness at the same time. Two techniques allowing to control the balance between phase separation and phase mixing have been proposed: the first one employs the MDs containing side groups[4] and the second one uses random polycarbonate copolymers containing different building units varying in the length of hydrocarbon chain and their proportion.[8,10,13,22–25]

Recently, we have prepared and characterized PC-PUs (from PC-based MDs of molecular mass around 1000, (T4671 and T5651), diisocyanate, chain extender, and in some cases layered nanofiller) prepared by one-step procedure in the form of sheets and free-standing films.[13,24] The ratio of OH groups in MD to that in butane-1,4-diol (BD), $[OH]_{MD}/[OH]_{BD}$), was set 1, 10, and ∞, varying hard-segment contents from 15 to 31 wt %. Besides excellent mechanical properties, the prepared elastomers and their nanocomposites showed an interesting phase behavior. We found that the nanofiller strongly interacts with hard domains influencing their melting temperatures, but it does not affect the glass transition temperature of soft domains. While the montmorillonite, Cloisite 15A, was found to bind and aggregate preferentially in hard domains, the organic-modified bentonite interacts also with soft segments, behaving as a kind of blending agent and influencing the end-use properties.[13] These observations call for further research and are the motivation for a more detailed and more comprehensive study (with HDI, butanediol, and in some cases bentonite for organic systems*). The molecular weight of MD in this study is higher, i.e., around 2000 (T5652, T4672, and T4692) which has a strong effect on the properties of final products (as it is shown in the second paper of this series devoted to mechanical and other functional properties).[28]

The objective of the present study is to investigate the effect of the poly(alkylene) carbonate structure, the PU composition (especially hard-segment contents), and the presence/absence of the nanofiller (bentonite) on the bottom-up built-up of self-assembled formations in PC-PUs in detail. In order to guarantee general validity of conclusions drawn from our model studies, the PC-PU elastomers were prepared from currently available, well-defined, and fully characterized starting materials. The $[OH]_{MD}/[OH]_{BD}$ ratio varied in the range 0.3–∞, corresponding to hard-segment contents variation from 8 to 34 wt %. HDI, BD, bentonite for organic systems (in some cases), and two kinds of polycarbonate MDs were used. They have almost identical MW, contents of hydroxyl groups, and number of carbonate units in the chain. However, they differ in the chemical constitution and therefore in the regularity of the copolymer chain: while the MD T5652 is composed of equal molar amount of even $[(CH_2)_6]$ and odd $[(CH_2)_5]$ units, the T4672 MD contains solely even units; the $[(CH_2)_4]/[(CH_2)_6]$ = C4/C6 ratio is 7 : 3 (or 9 : 1 in the case of T4692).

In order to describe the behavior of PU copolymers from the nano-to-micrometer scale level, appropriate analytical methods were used: spectroscopy techniques describing process on the segmental and molecular level, scattering techniques evaluating the degree of the self-assembly of organized structures mainly on the nanometer scale and microscopy

*Due to rather limited tensile properties of nanocomposites made from macrodiols MW 1000 containing Cloisite 15 A (compared with bentonite for organic systems),[13] nanofiller 15 A was not used in this study.

techniques, enabling the characterization on the nanometer up to micrometer scale. The second part of the study (Paper II, submitted to *Journal of Applied Polymer Science*) will be focused on the macroscopic thermal, thermomechanical, mechanical, and gas transport properties).[28] In both papers, the comparison with relevant published data is discussed.

EXPERIMENTAL

Materials

All-aliphatic polycarbonate MDs with molecular weight of about 2000 (PCDL T5652, PCDL T4672, and PCDL T4692; marked as 5652, 4672, and 4692) were kindly provided by Asahi Kasei Chemical Corporation (Tokyo, Japan). (All MDs were prepared by random copolymerization of butanediol (resp. pentanediol) and hexanediol with ethylene carbonate. The currently used nomenclature is: first two numbers are numbers of methylene units in the copolymer (C4 and C6 resp. C5 and C6), the third is the molar ratio of the butane (resp. pentane) units, and the last number indicates the thousand digits the molecular weight of PC diol.[8] For example, 5652 is the MD of MW of about 2000, containing equal molar ratio of pentane, C5, and hexane, C6, units).[†] The characteristics of MDs were given by the supplier: 5652 OH value: 57.0 mg KOH/g, water content: 0.0043 wt %, viscosity at 50°C: 9970 mPa s; 4672 OH value: 54.2 mg KOH/g, water content 0.0077 wt %, viscosity at 50°C: 18,300 mPa s; 4692 OH value: 55.8 mg KOH/g, water content 0.0185 wt %, viscosity at 70°C: 6410 mPa s. HDI, BD (chain extender), and the catalyst, dibutyltin dilaurate (DBTDL), all Fluka, were used as received. The catalyst solution was prepared in oil Marcol (20%). The modified bentonite (bentonite for organic systems, BO, Fluka, Buchs, Schweiz) was used as filler.

Preparation procedure

The PU sheets were prepared by one-step technique. The isocyanate index, r = [NCO]/[OH] was kept constant 1.05 in all cases. The ratio $R = [OH]_{MD}/[OH]_{BD}$ varied from 0.3 to ∞. $R = \infty$ means PU samples prepared without any chain extender (BD). Catalyst concentration, c_{DBTDL}, was kept at 0.005 wt %. The mixture containing MD, chain extender, and catalyst was degassed. Then diisocyanate was added in the reaction mixture, mixed, again degassed, and poured into Teflon molds. The samples containing the filler (PU-clay nanocomposites) were prepared by the same procedure, when a full dispersion of nanofiller (bentonite, BO) was achieved by one day swelling in MD and butanediol mixture, and by subsequent brief stirring for 10 min of the mixture, prior to addition of isocyanate. The preparation procedure for film is the same like for sheets, but the final mixture was finally spread on polypropylene sheet (instead putting into Teflon molds). The constant layer thickness was obtained using a ruler. All samples (sheet- or film-shape) were kept in nitrogen atmosphere at 90°C for 24 h. (The final thickness of PU sheets was 2 ± 0.1 mm and PU films 0.5 ± 0.05 mm).

For all PC-PU samples prepared, uniform codes were used: MD type/R/wt % of BO/wt % of HS. (For example code 4672/10/1/9 means PU prepared from 4672 MD at ratio R =10 ($R = [OH]_{MD}/[OH]_{BD}$), containing 1 wt % of bentonite and having 9 wt % of HS). Sample composition and codes are summarized in Table I, columns 1–5.

Experimental methods

Solid-state NMR spectroscopy

^{13}C-CP/magic angle spinning (MAS) NMR spectra were recorded on a Bruker AVANCE 500 spectrometer (Larmor frequencies $\nu^{13}C$ = 125.783 MHz) using a 4 mm MAS probe. The spinning speed of rotor sample was 11 kHz. The number of scans for the accumulation of ^{13}C CP/MAS NMR spectra was 1536, repetition delay of 4 s, and spin lock of 1 ms. During detection, a high-power dipolar decoupling was used to eliminate strong heteronuclear dipolar coupling. The isotropic chemical shift of ^{13}C scale was calibrated with glycine as external standard (176.03 ppm to carbonyl signal).

Fourier transform infrared spectroscopy

The Fourier transform infrared spectroscopy (FTIR) spectra were recorded on a Perkin–Elmer Paragon 1000PC FTIR spectrometer using the reflective attenuated total reflection (ATR) technique Specac MKII Golden Gate Single Reflection ATR System with a diamond crystal with the angle of incidence 45°. All spectra were measured at wavenumber range 4400–450 cm^{-1} with resolution 4 cm^{-1} and with 16 scans. Software Spectrum v2.00 was used for processing the spectra. The samples were directly put on the diamond crystal and measured.

Small-angle X-ray scattering

Small-angle X-ray scattering (SAXS) experiments were performed using a three pinhole camera (Molmet/Rigaku) attached to a multilayer aspherical optics (Osmic Confocal Max-Flux) which monochromatizes and concentrates the beam of a microfocus X-ray tube (Bede) operating at 45 kV and 0.66 mA (30 W). The camera was equipped with a multiwire,

[†]All PC diols used have by implication of the composition and the molecular weight very similar number of carbonate groups distributed in the macrodiol chain.

TABLE I
Codes, Composition, Position of SAXS Peaks and Degree of Crystallinity for PC-PUs and Their Nanocomposites

Code	PC diol	R[a]	BO (wt %)	HSC (wt %)	$SAXS_{max1}$ (nm)	$SAXS_{max2}$ (nm)	Degree of crystallinity (%)
5652/0.3/0/35	5652	0.3	0	35.4	14.0		10
5652/0.5/0/27	5652	0.5	0	26.9	14.1	–	14
5652/0.5/1/27	5652	0.5	1	26.8	14.4	3.2	12
5652/1/0/19	5652	1	0	18.7	15.7		9
5652/1/1/19	5652	1	1	18.6	15.8	3.5	14
5652/1/2/19	5652	1	2	18.5	NA[b]	NA[b]	NA[b]
5652/2/0/14	5652	2	0	13.9	12.0	–	0
5652/10/0/9	5652	10	0	9.2	10.0		0
5652/∞/0/8	5652	∞[c]	0	8.4	0		0
4672/0.3/0/34	4672	0.3	0	34.2	14.0		9
4672/0.5/0/26	4672	0.5	0	25.9	15.5	–	15
4672/0.5/1/26	4672	0.5	1	26.0	15.8	3.2	14
4672/1/0/18	4672	1	0	17.8	17.9		4
4672/1/1/18	4672	1	1	17.7	18.7	3.3	8
4672/2/0/13	4672	2	0	13.1	14.4	–	0
4672/10/0/9	4672	10	0	8.9	10.0		0
4672/10/1/9	4672	10	1	8.9	0	3.5	0
4672/∞/0/8	4672	∞[c]	0	8.0	0		0
4692/1/0/18	4692	1	0	18.2	13.4	–	10

[a] $R = [OH]_{MD}/[OH]_{BD}$.
[b] NA = not analyzed.
[c] Prepared without any BD. (HSC = $(m_{HDI} + m_{BD})/(m_{HDI} + m_{BD} + m_{MD})$, where m is mass of the relevant component; expressed in wt %).

gas-filled 2D detector with an active area diameter of 0.2 m (Gabriel design). In the high resolution mode, the sample to detector distance was 2.24 m and in the low resolution mode 0.41 m, so that total interval from 0.043 to 10.5 nm^{-1} of the scattering vector magnitude $q = (4\pi/\lambda)\sin\theta$, where $\lambda = 1.54$ Å is the wavelength and 2θ is the scattering angle, could be reached. Calibration was performed using AgBehenate sample. If peaks were present, their positions were employed to obtain characteristic length D according to Bragg's law, $D = 2\pi/q$. Scattering intensities were put on absolute scale using a glassy carbon standard. Typical counting times were 3600 or 10,000 s.

Wide-angle X-ray diffraction

Wide-angle X-ray diffraction (WAXD) measurements were conducted with the use of the HZG/4A powder diffractometer (Seifert GmbH, Germany). The peak positions were employed to obtain periodicities according to Bragg's law, $d = \lambda/2\sin\theta$, where λ is the X-ray wavelength ($\lambda_{CuK\alpha} = 0.154$ nm) and 2θ is the scattering angle. The degrees of crystallinity C_r were calculated with help of integral intensities diffracted by crystalline C and amorphous A part of materials according to relation $C_r = C/(C + A)$.

Atomic force microscopy

Investigation of the surface topography was done by a commercial atomic force microscope (MultiMode Digital Instruments NanoScopeTM Dimension IIIa), equipped with the SSS-NCL probe, Super Sharp Silicon™-SPM-Sensor (NanoSensors™ Switzerland; spring constant 35 Nm^{-1}, resonant frequency ≈ 170 kHz). Measurements were performed under ambient conditions using the tapping mode atomic force microscopy (AFM) technique. The scans covered the sizes from 0.3 × 0.3 to 30 × 30 μm. The AFM images of either the fracture areas of PC-PU sheets after previous freeze-fracturing at the temperature of liquid nitrogen (F) or the cut area after cutting on an ultramicrotome with cryo attachment at −110°C (C) were measured in order to evaluate the inner arrangement in the bulk system, mainly the size and shape of hard domains.

Transmission electron microscopy

Ultrathin sections of the films were cut on an ultramicrotome with cryo attachment (Ultracut UCT, Leica) at −110°C. The sections were transferred to supporting Cu grids and observed using a transmission electron microscope (JEM 200CX, Jeol) at 100 kV. The transmission electron microscopy (TEM) photographs were digitized with a digital camera (DXM1200, Nikon). The brightness and contrast of the digitized TEM photographs were adjusted using standard software.

RESULTS AND DISCUSSION

In this work, all-aliphatic PC-PU elastomers and their nanocomposites with organic-modified

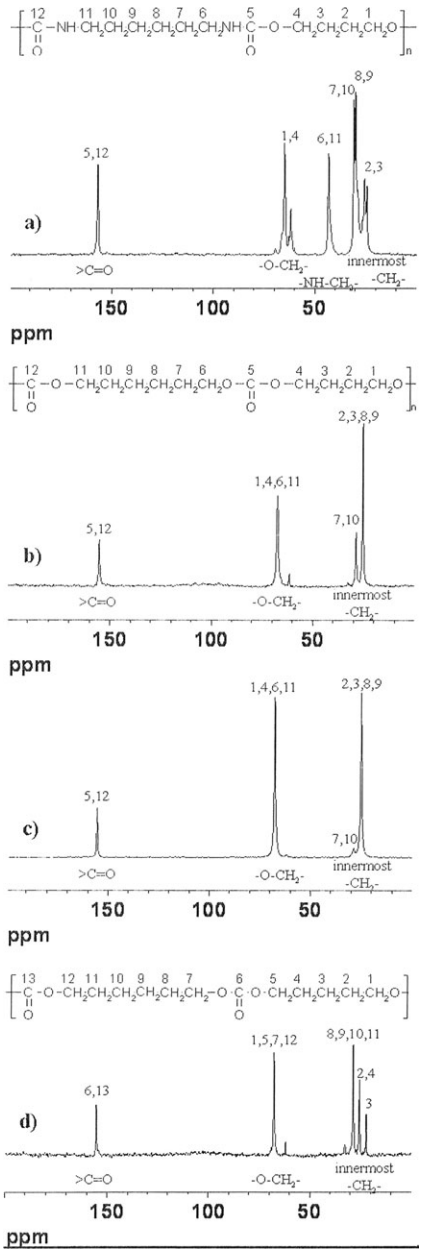

Figure 1 NMR1: ^{13}C-CP/MAS NMR spectra and structural formulas of: HDI/BD homopolymer (a), and MDs: 4672 (b), 4692 (c), and 5652 (d). (Structural units of 4672 and 4692 MDs are identical).

bentonite were synthesized in one-step procedure. As all components are bifunctional, linear PU chains are composed of alternating elastic soft segments originating from the aliphatic polycarbonate diol component (MD, with MW ca., 2000), and more rigid polar HS formed by HDI/BD building units which have the tendency for ordering to hard segment domains (HSD) and form semicrystalline structures if the hard segment content (HSC) is high enough. HS arising from diisocyanate and chain extender feature by formation of strong physical networks by H-bonding among —NH and —C=O groups in urethane (—NHCOO—) units resulting in material reinforcement. Moreover, in our case, (secondary) H-bonding via —NH groups of urethane units and carbonate carbonyl groups of MD (hard-soft segment H-bonds) is necessary to take into account, because all MDs contain regularly distributed carbonate (O—CO—O) groups in PC diol (and hence also in PU) chain.

We have studied the bottom-up self-assembly of building units in polyurethane elastomers, i.e., the formation of self-assembled domains during the synthesis, their sizes and inner structure (ordering of chains, content of H-bonds), their effect on the mechanical and other properties and particularly the relationship between chemical nature and structure of starting materials on one hand and the morphology and functional properties of final products on the other hand. For this purpose, the combination of spectroscopies (solid-state NMR and FTIR), scattering (small- and wide-angle X-ray), microscopy (atomic force and transmission electron) and other analytical methods was used.

Solid-state NMR spectroscopy

Solid-state NMR spectroscopy was used for studying the structure and ordering of prepared

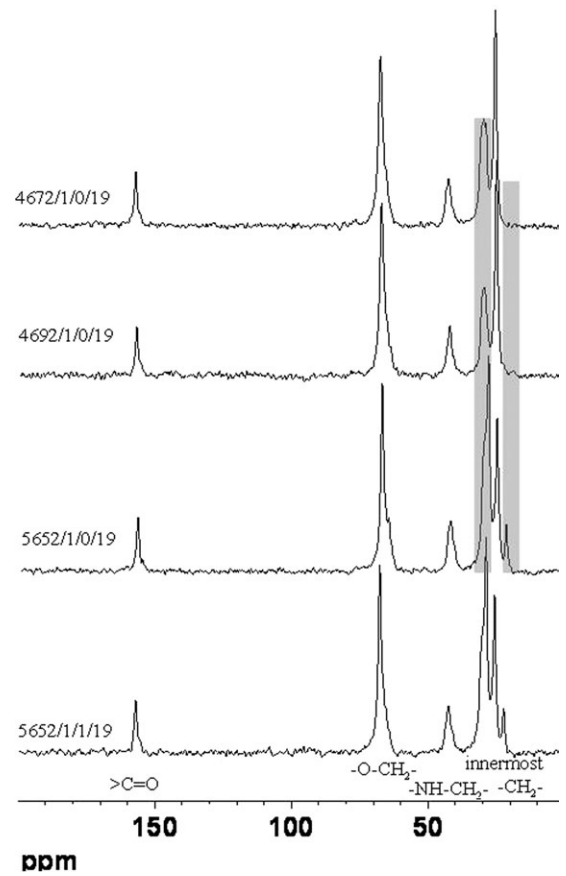

Figure 2 ^{13}C-CP/MAS NMR spectra of PU and PU nanocomposite made from HDI, BD, and different MDs at R = 1.0. (For code description, see Table I).

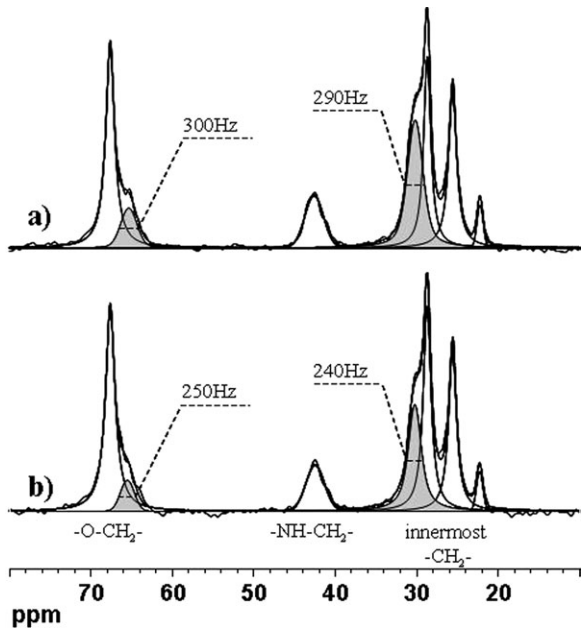

Figure 3 The comparison of ^{13}C-CP/MAS NMR spectra of PC-PU (5652/1/0/19), (a) and PC-PU nanocomposite (5652/1/1/19), (b) with the deconvolution of all peaks.

nanostructured PUs. At first, we performed the characterization of (i) building units of "hard segments" (HDI/BD homopolymer) and soft segments (MDs 4672, 4692 and 5652)—Figure 1, and (ii) polyurethane elastomers prepared from different MDs and PU elastomer filled by clay (BO)—Figure 2.

All peaks of starting materials labeled in Figure 1 have been assigned using liquid NMR techniques (^{1}H–^{1}H COSY and ^{1}H–^{13}C HETCOR). ^{13}C-CP/MAS NMR spectra of starting MDs fit well to the structure of building units. The differences in intensities of peaks 7 and 10 in 4672 and 4692 MDs correspond to the difference in molar ratio of C4 and C6 units. The observed differences in half-width (HW) of signals indicate that MDs 4672 and 4692 are more rigid (on the molecular level) than MD 5652—the signals of 5652 are narrower than that of 4672/4692: HW are narrower by 20 Hz at 25 ppm and by 35 Hz at 68 ppm.

NMR data illustrated in Figure 2 show that all reactions used led to a high degree of conversion. The differences of peaks of innermost —CH_2— groups in the region 20–35 ppm are shown in highlighted areas. The ^{13}C-CP/MAS NMR spectra confirm the purity of the components used (MDs, butanediol, isocyanate) and their full incorporation in the PU polymers. No N=C=O carbonyl peak of unconverted isocyanate (near 120 ppm) was observed (although this signal is typically weak in the ^{13}C-CP/MAS NMR, a very precise proof of full NCO conversion was provided by the FTIR spectroscopy by the absence of very characteristic and strong NCO peak—see Chapter "Fourier transform infrared spectroscopy"). The differences in spectra (peaks at 26 and 28 ppm) are caused only by the difference in MD structures: sample 4692/1/0/19 has lower ratio of C6 units in the copolymer (C4 : C6 = 9 : 1) than 4672/1/019 (C4 : C6 = 7 : 3; in accordance to producer data). In the case of PC-PU (5652/1/0/19) and analogue PC-PU nanocomposite (5652/1/1/19) in Figure 2, all peaks are nearly identical due to identical composition of both samples. However, there are differences in the intensity and half-width of peaks in the region of 20–70 ppm. The ^{13}C-CP/MAS NMR spectra in this region including the deconvolution of all peaks are given in Figure 3. Both peaks at 35 and 65 ppm highlighted in Figure 3 are by about 50 Hz narrower in the nanocomposite compared with the nanofiller-free analogue, which implies that system 5652/1/1/19 is more ordered than 5652/1/0/19 one. We assume that the presence of BO particles can partially restrain the formation of hydrogen bonds in the PU matrix in 5652/1/1/19 sample as compared with 5652/1/0/19. No pronounced changes of all signals belonging to MD were found which means that bentonite influences preferably the hard-segment region compared with the soft-segment one.

Fourier transform infrared spectroscopy

FTIR was used to study chemical structure of starting components and their PU products, isocyanate group conversion, and especially hydrogen bond formation in PC-PU films built-up from different PCD and containing different HSC.

Representative infrared spectra of 5652/1/0/19 sample with two inserts containing expanded N—H stretching from 3200 cm^{-1} to 3500 cm^{-1} and C=O carbonyl stretching region from 1600 cm^{-1} to 1800 cm^{-1} is shown in Figure 4. Positions of the absorption bands belonging to the specific functional groups were similar for all obtained samples (i.e., depending neither on MD constitution nor HSC). No isocyanate peak at about 2270 cm^{-1} was observed in all IR spectra, indicating no residual isocyanate groups and full NCO conversion. The absorption peaks at about 2900 cm^{-1} and 2850 cm^{-1} are associated with C—H symmetry and asymmetry stretching vibrations of the aliphatic —CH_2— groups. The peaks in 5652-, 4672-, and 4792-based PU differ mainly in the intensity of the peaks due to their somewhat different chain constitutions, see Experimental. The peak at 1532 cm^{-1} is the joint frequency of the bending vibration of N—H bond and stretching vibration of the amidic C—N. The 1462 cm^{-1} peak is the symmetrical bending vibration of CH_2. The strong and sharp absorption peak at 1238 cm^{-1} corresponds the stretching vibration of the C—O of the carbonate group; 1063 cm^{-1} is the stretching vibration of the

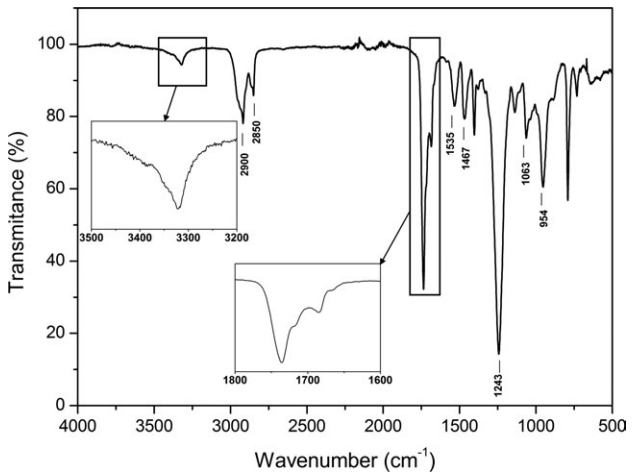

Figure 4 FTIR spectra of PC-PU film 5652/1/0/19.

C—O—C in urethane units; the 951 cm^{-1} peak is the symmetry stretching vibration of the C—O—C in carbonate.

In order to assign peaks belonging to "free" and H-bonded carbonyls originating from polycarbonate and urethane groups, IR spectra of MD 5652 (as a representative of soft segment) and "pure" hard segment (i.e., HDI and BD product) were recorded. Carbonyl stretching regions from 1600 to 1800 cm^{-1} of "pure" hard segment and 5652 MD are shown in Figure 5(a). The deconvolution of the carbonyl stretching region of "pure" hard segment [Fig. 5(b)] revealed that this band is composed of at least five peaks: peak around 1725 cm^{-1} (band I) is attributed to the free carbonyl groups whereas two other peaks at about 1708 cm^{-1} (band II) and 1695 cm^{-1} (band III) are assigned to H-bonded carbonyl groups in the amorphous phase. Remaining two peaks at 1680 cm^{-1} (band IV) and 1664 cm^{-1} (band V) pertain to H-bonded carbonyl groups in the crystalline (ordered) phase. The peaks at 1680 cm^{-1} and 1664 cm^{-1} are present not only in the "pure" hard segment but they were also detected in PU samples containing more than 14% of HSC, that means in all PU samples being semicrystalline (for details, see the following chapter, SAXS and WAXD experiments). The peak at 1736 cm^{-1} belonging to the pure 5652 MD is ascribed to the "free" C=O from carbonate groups.

We assume that the splitting of IR peaks in studied materials is due to different possibilities of H-bond formation and can be rationalized as follows: Two —O—CO—NH— groups from two different polyurethane chains can form either one hydrogen bridge as depicted in Scheme 1(a) or an 8-member ring containing two hydrogen bonds as shown in Scheme 1(b). Moreover, a slightly different H-bond can form between one —O—CO—NH— and one —O—CO—O group [Scheme 1(c)].

The carbonyl stretching region between 1600 and 1800 cm^{-1} of PU samples with different HSC is shown in Figure 6. The peaks around 1736 cm^{-1} and 1718 cm^{-1} are ascribed to the "free" and H-bonded carbonyls from the carbonate groups. However, the H-bonded "carbonate" peak at about 1718 cm^{-1} can be overlapped by peaks originating from "free" and H-bonded C=O urethane groups in the amorphous phase. The H-bonded carbonyl groups from the urethane in the semicrystalline state are present around 1683 cm^{-1} and 1667 cm^{-1}. On condition that the carbonyl stretching region of the sample without any chain extender is analyzed (5652/∞/0/8; curve 4 in Fig. 6) it can be noticed that only negligible amount of H-bonded urethane groups in the crystalline (ordered) state is formed. H-bond formation takes place with carbonate carbonyls as well as with urethane groups but without any long-range ordering. As it is clearly seen in Figure 6, an increase in HSC results in increase of the amount of hydrogen bonds which (as shown by scattering techniques—see later) induces the formation of crystalline domains dispersed in the amorphous phase.

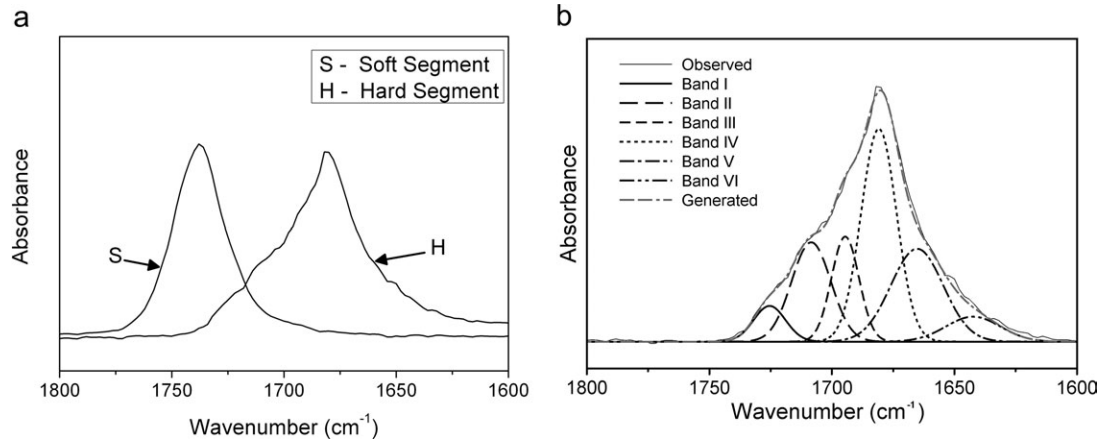

Figure 5 (a) FTIR-spectra of polycarbonate diol 5652 (S) and HDI/BD homopolymer (H); (b) The deconvolution of the carbonyl stretching region of the hard segment (H).

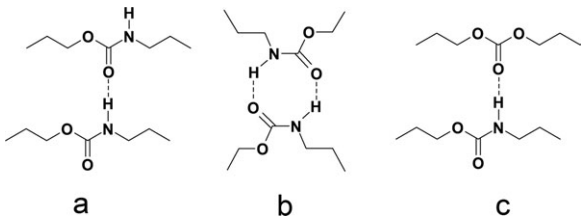

Scheme 1 Possible H bonds in urethane units (a,b) and urethane-carbonate groups (c) in HS (a,b) and in polyurethane elastomers (a,b,c).

Expanded N—H stretching region of the PU samples with different HSC is shown in Figure 7. The deconvolution led to the following peaks: The infrared bands at 3430–3460 cm^{-1} and 3318–3323 cm^{-1} are assigned to the N—H stretching vibrations of the "free" and H-bonded N—H groups. (The HSC increase, and hence the increase of number of urethane groups, enlarges the total area and the intensity of relevant bands). Peaks at 3387–3393 cm^{-1} and at 3245–3251 cm^{-1} present in all measured samples are attributed to the Fermi resonance of N—H fundamental stretching vibration with the overtone of carbonyl C=O carbonate stretching vibrations. Spectra of PU samples containing more then 14% of hard segment contain two additional peaks: at 3345 cm^{-1} and 3290 cm^{-1} which are absent in samples with lower HSC.

SAXS and WAXD experiments

SAXS experiments were used to investigate microphase-separated state. A number of papers indicates that homopolymers made from HDI and BD acquire folded-chain conformation that is also often present in HDI/BD-based PUs.[29,30] Molecular modeling confirmed possible self-assembly of HS in aliphatic PU in stacked lamellar patterns inside the crystallite.[30]

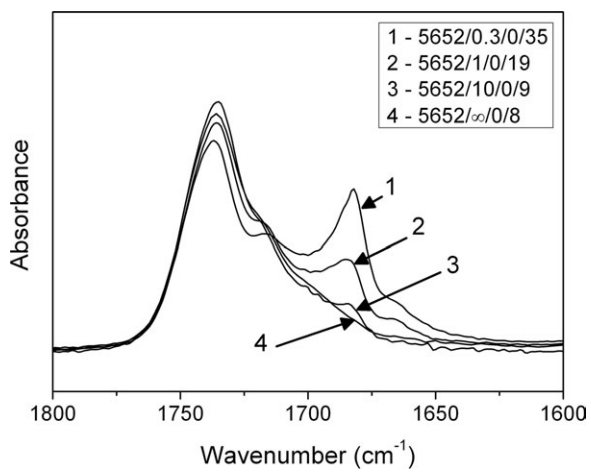

Figure 6 FTIR spectra of carbonyl stretching region of 5652-based PC-PUs with different HSC (For code description, see Table I).

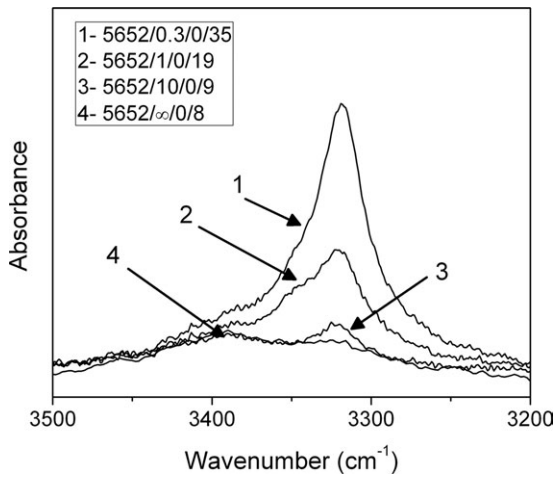

Figure 7 Expanded FTIR spectra of N—H stretching region of PC-PUs with different HSC. (For code description, see Table I).

Important feature of aliphatic PUs is a closer proximity of the PU chains in hard domains as compared with aromatic PUs; the HDI/BD proximity allows for further self-assembly of HS via H-bonding into domain/cluster patterns.[30]

SAXS profiles of 5652- and 4672-based PC-PUs and their nanocomposites are shown in Figure 8. Both series have similar trends: As expected, PC-PUs prepared without any chain extender show no scattering peaks. All other PUs exhibit scattering peaks the shape and the position of which depend on HSC. The values of interdomain spacing of HSD in 4672- and 5652-based PC-PUs were calculated from the peak position, they span from 10 nm to 18.7 nm and they are given in Table I, 6th column. The self-assembly of HDI/BD-based HSD leading to folded-chain conformations is anticipated in studied PC-PUs, as the values of interdomain spacing given in Table I correspond well, e.g., to SANS data by Mishra et al. for aliphatic PUs prepared from polyether diol (MW about 2900), HDI and BD (11.6–16.2 nm),[30] or to PES- (MW about 2000) and HDI/BD-based aliphatic PUs (16.6 nm).[29] However, the trends reported in the literature are not uniform: while characteristic lengths of interdomain spacing in PES-based PUs decreases with increasing HSC suggesting higher compactness of crystallites with increasing H-bonding extent,[30] the interdomain spacing in polyether-based PUs was reported practically independent on HSC.[29] The systems studied in this article show even more complex behavior: the interdomain spacing passes a maximum (15.7 nm for 5652-based PUs and 17.9 nm for 4672-based samples; both at $R = 1$). For the highest, about 35 wt % HSC ($R = 0.3$), the interdomain spacing decreased to 14 nm in both series. The spacing reduction could be a result of increased compactness of crystallites[30] and

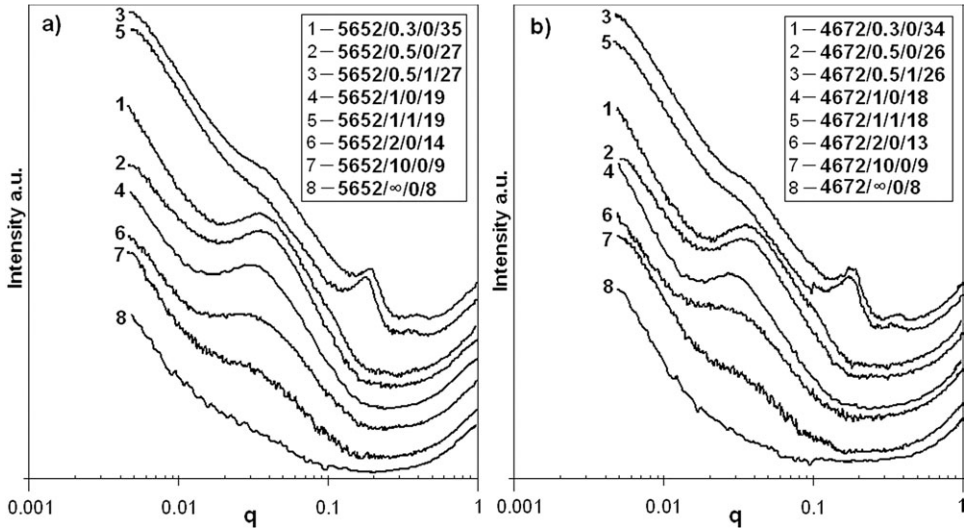

Figure 8 Scattering curves for 5652- (a) and 4672-based PU series (b). (For code description, see Table I).

of increasing rigidness of PC-PU chains due to strong secondary forces of H-bonding among NH— of urethane groups (HS) with carbonate C=O groups belonging to soft-segments. The reduction of the interdomain spacing for samples with higher ratio *R* can be caused by relatively low HSC (8–14 wt %).

If BO particles are present, the scattering peaks in nanocomposites (compared with their BO-free analogues) are much broader, less pronounced, and they are mostly shifted to higher values of interdomain spacing, see Table I. That means that the lamellar patterns in the presence of BO lamellae correspond to lower level of lamellar ordering. SAXS profiles for all nanocomposites are very similar, independent on the ratio *R*, showing two additional peaks at about 3.5 nm and at 1.8 nm. These two peaks correspond to well ordered lamellar structure of BO particles intercalated by PU matrix with the periodicity of about 3.5 nm (Table I, 7th column).

WAXD

The degree of crystallinity was investigated by WAXD. The WAXD patterns for 5652- and 4672-based PU elastomers and their nanocomposites are shown in Figure 9. WAXD patterns for both series (4672 and 5652) are very similar: The gradual development of crystallinity with increasing content of HS is very well visible; starting from fully amorphous materials ($R = 10$ and ∞) passing through those with developing crystalline peaks ($R = 1$) up to semicrystalline products with three pronounced crystalline peaks ($R = 0.5$ and 0.3). The tendency to

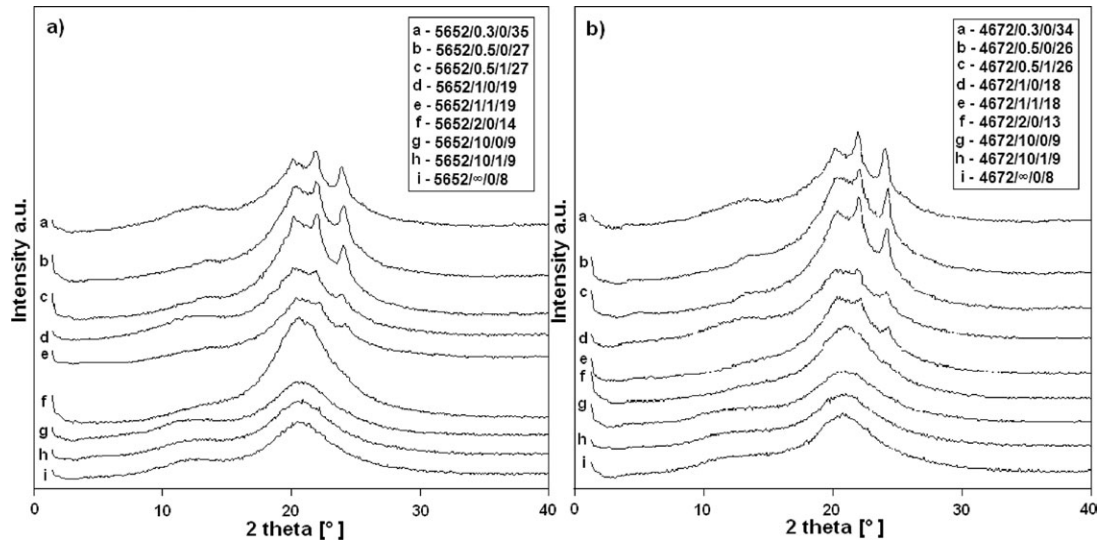

Figure 9 WAXD patterns of 5652-based PC-PUs (a) and 4672-based PC-PUs (b). (For code description, see Table I).

ordering is stronger in the 4672 matrix, because MD 4672 is noted for higher regularity of the chain compared with 5652 one. The observed diffraction patterns exhibit broad (amorphous) peaks near $2\theta = 21$ °, corresponding to the distribution of distances of neighboring polymer chain segments. Besides this diffraction peak, another shallow maximum is observed near 13°; this is assigned to the internal structure of the polycarbonate chains, namely to the average distance of the carbonate groups. Separated sharp narrow peaks between 20° and 24° (values for most samples in both series: 20.1°, 22°, and 24°) correspond to crystalline domains. The appropriate separation of both types of signals gives the degree of crystallinity summarized in Table I, 8th column. The crystallinity (for PUs with HSD higher than about 15 wt %) depends on the HSC; it spans from 4 to 15%. The highest crystallinity was not found for PC-PUs with the highest HSC (34–35%), but for samples containing 26–27% HSC. This slightly surprising finding is probably due to high stiffness of PU chains at the highest HSC, which can hinder ordering of PU segments in organized crystalline domains. Strong secondary forces of H-bonding among NH— of urethane groups (HS) with C=O groups of polycarbonate part (SS) resulting in the increasing of chain rigidity can be also taken into consideration.

For given HSC, systems with BO particles have slightly higher degree of crystallinity compared with their BO-free analogues (see Table I), that implies better organization of nanocomposites compared with pure PC-PU matrix, which is in accordance with solid-state NMR experiments. WAXD was also used for the detection of lamellar periodicity of BO particles in PC-PU nanocomposites. While original BO powder shows diffraction maximum near 1.1 nm, PC-PU nanocomposites exhibit two orders of maxima corresponding to well ordered lamellar structure with periodicity between 3.2 and 3.5 nm implying intercalation of PU matrix between BO lamellae.

The comparison of PC-PUs containing MD building blocks of MW about 2000 $(PC\text{-}PU)_{2000}$ with analogous systems based on MDs with half MW (1000), $(PC\text{-}PU)_{1000}$,[13] but otherwise identical chemical constitution, revealed the similar trends for systems with identical ratio R: all PU prepared at $R = 1$ are semicrystalline, whereas PUs with $R = 10$ or ∞ are amorphous. However, $(PC\text{-}PU)_{1000}$ elastomers with identical composition have about 1.7 times higher HSC than analogous $(PC\text{-}PU)_{2000}$. When PU samples with similar HSC (e.g., semicrystalline 5652/1/0/19; crystallinity 9%, with amorphous 5651/10/17[13]) are compared, the tendency of enhanced phase mixing and worse structural ordering in samples with shorter building MD units is evident. All PU nanocomposites show a higher degree of ordering than their nanofiller-free analogues, neither dependent on the MD chain constitution nor its length.

When comparing our results with WAXD results of Kojio et al.,[8] the influence of the diisocyanate type on the ordering and crystallinity of PU chains can be well demonstrated: PC-PUs with codes 4672/1/0/18 and 4672/0.3/0/34 have very similar composition to samples 4672PU2 and 4672PU3[8]; the only difference is the use of HDI (in our case) and MDI.[8] When compared 4672/1/0/18 and 4672/0.3/0/34 WAXD patterns (Fig. 9) with 4672PU2 and 4672PU3 ones (Fig. 3 in Ref. 8), a significantly higher degree of the ordering (crystallinity) was found for HDI/BD domains than for MDI/BD ones. This can be explained by different proximity of PU chains containing HDI/BD or MDI/BD domains.[30]

AFM and TEM analyses

AFM was used to study the size and shape of hard domains in the PU elastomers prepared. In our recent papers, the surfaces of PC-PU films[22] or the freeze-fractured cross-sections of PC-PUs prepared in the form of sheets[13] were analyzed by AFM to investigate the hard/soft segment morphology. In this study, the freeze-fracture (*F*) was used as well and the surfaces of PU sheets cut at −110°C (*C*) were also investigated to test the influence of the preparation of the surface for imaging on AFM results.‡ A series of the height and phase AFM images for selected 5652-based PC-PUs is shown in Figures 10(a–g) and 11 (a–j).

3D height reliefs of 10×10 μm^2 area of freeze-fractured (*F*) samples 5652/0.3/0/35, 5652/1/0/19, and 5652/∞/0/8 are shown [Fig. 10(a–c)] together with relevant 2D phase images [Fig. 10(d–f)]. While the sample 5652/∞/0/8 (amorphous according to WAXD) shows a flat and homogeneous surface, the semicrystalline samples 5652/0.3/0/35 and 5652/1/0/19 show height and heterogeneity differences on the nm and μm level. PUs containing 1 and 2 wt % of BO (5652/1/1/19 and 5652/1/2/19) have very similar height reliefs like BO-free PU analogue (5652/1/0/19); the addition of BO only slightly increases surface roughness (see Table II). It is evident from Table II that the roughness depends mainly on HSC (the higher HSC, the higher roughness) whereas the influence of nanofiller concentration on the roughness is very small. The spherullite structures of about 10 μm size in semicrystalline samples are well detectable by using TEM and AFM analyses; Figure 10(g) (AFM) and Figure 10(h) (TEM).

‡Similarly to our previous study (Fig. 2 and Table I in Ref. 22), surface patterns of the films were regular and relatively smooth (mean roughness of mostly 10^1 nm order) and practically the same for 5652-, 4672- and 4692-based samples. In this way, surface analysis of films is not shown in this paper.

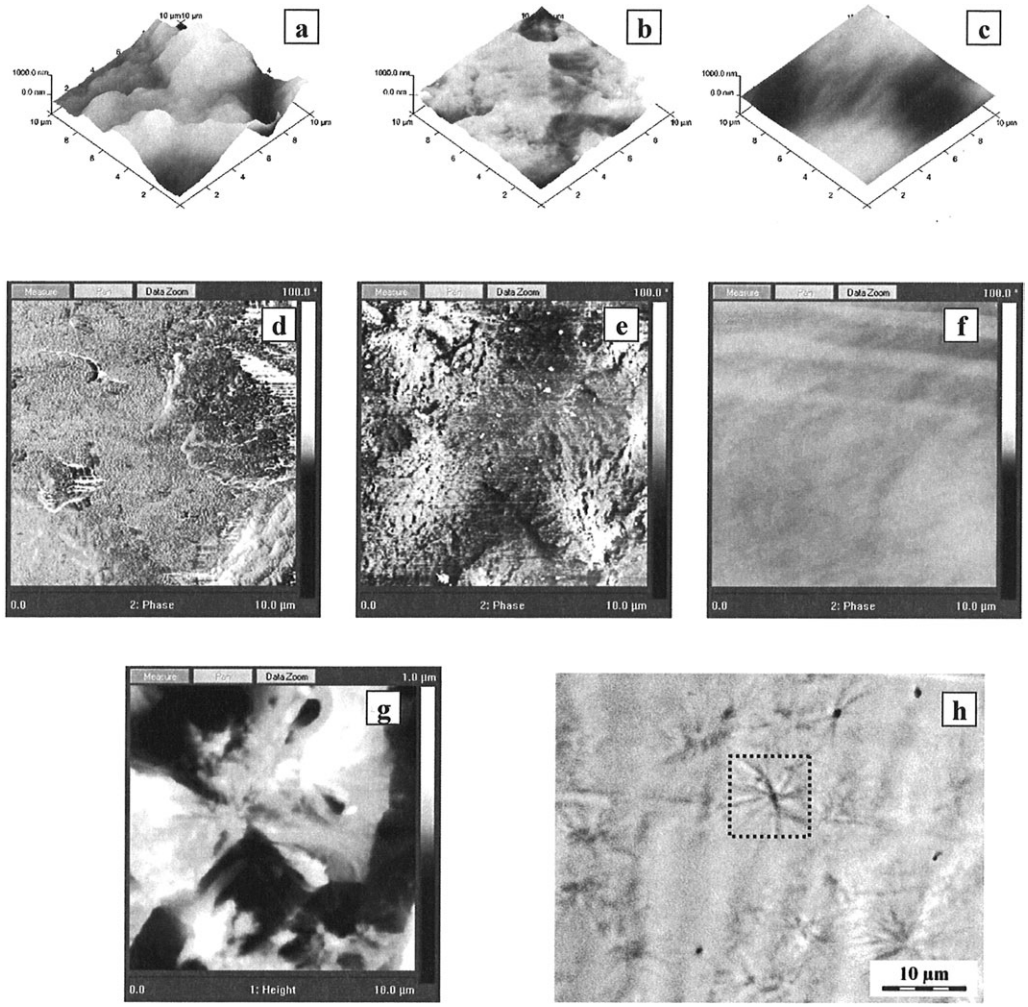

Figure 10 3D Height (a, b, c), 2D phase (d, e, f), 2D height (g) AFM images, and TEM microphotographs (h) of PU samples: 5652/0.3/0/35 (a, d), 5652/1/0/19 (b, e, g, h) and 5652/∞/0/8 (c, f). (For code description, see Table I). AFM *z* or black-and-white color scale: 1000 nm for height, and 100° for phase image. Square in TEM image: highlighting of 10 μm^2 area.

Scanning 1 × 1 μm^2 areas enabled the study of heterogeneities on the nm level. The influence of sample preparation on AFM measurement (*C*, *F*) was also studied. Freeze-fractured sample (*F*): Sample 5652/∞/0/8 shows a flat surface [Fig. 11(a)] with slight regular (nm-size) nanoheterogeneities (detected by phase shift) [Fig. 11(b)]. If two PUs with $R = 1$, one without BO and the other with 2 wt % of BO, i.e., 5652/1/0/19 and 5652/1/2/19 are compared, the surface topography does not differ significantly [Fig. 11(c,e)]. Both phase images show rod-like nanoheterogeneities, of 10^0 nm in width and 10^0 to 10^2 nm in length. Moreover, in sample 5652/1/1/19, BO particles of size 100–250 nm are clearly visible [Fig. 11(e,f)], mainly in phase image [Fig. 11(f)]. Cut samples 5652/1/0/19 and 5652/1/1/19 (C), shown in Figure 11(g–j) differ from the fractured samples (*F*) in height, but mostly in phase images; they seem to be more homogeneous than the broken ones. However, on condition of sufficient phase resolution (color scale 5° (*C*) vs. 100° (*F*)), very regular and smooth but distinct heterogeneities of units of nm size are also detected [Fig. 11(h,j)]. BO particles are also well visualized [Fig. 11(i,j)] but they are less distinct compared to freeze-fractured samples [Fig. 11(e,f)] because BO particles are in this case "covered" by PU matrix.

In PUs with very low HSC (5652/1/∞/8 (*F*)) their height and phase images are almost identical like 5652/1/0/19 (*C*) [cf. Fig. 11(a) vs. Fig. 11(g) and Fig. 11(b) vs. Fig. 11(h)]. In all cases, all 1 × 1 μm^2 surfaces are very flat: RMS and mean roughness are on nm scale and R_{max} on 10^1 nm level (Table III).

The difference between images of "*F*" and "*C*"—prepared surfaces can be caused by the difference in their formation: While the freeze-fractured area is predetermined by sample imperfectness, nanoheterogeneities, etc., which control the fracture, the cryocut sample surface is created by the cutter position and motion. Hence the HSD on µm scale is better

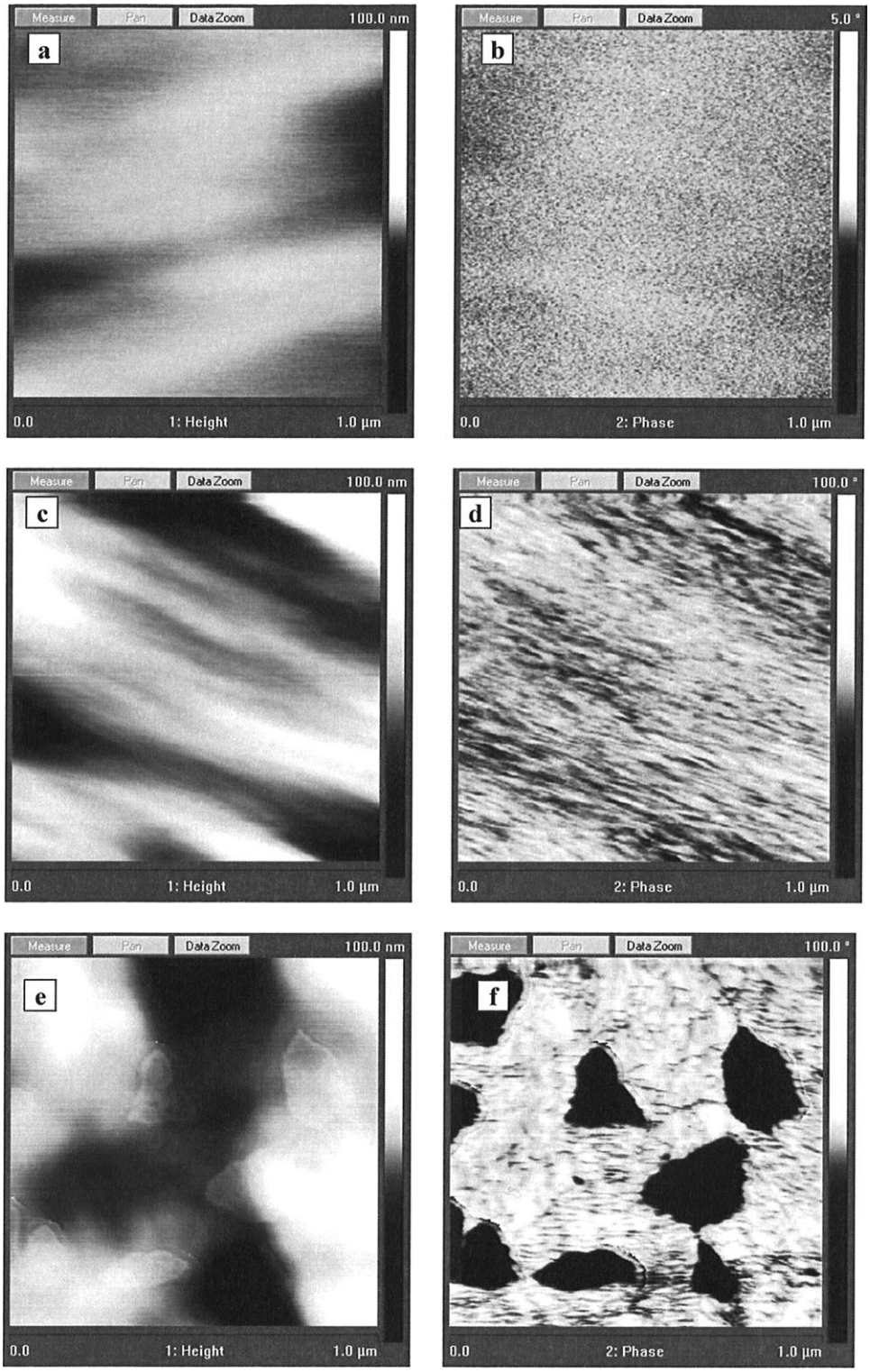

Figure 11 2D Height (a, c, e, g, i) and 2D phase (b, d, f, h, j) AFM images of PU samples: 5652/∞/0/8 (a,b), 5652/1/0/19 (c,d,g,h), 5652/1/2/19 (e,f,i,j). Images of freeze-fractioned (*F*) samples (a–f); images of cut (*C*) samples (g–j). (For code description, see Table I). Black-and white color scale: 100 nm for height images (a,c,e,g,i), 100 deg (d,f) and 5 deg (b,h,j) for phase images.

seen on broken samples (*F*), while small heterogeneities detection on nm size have been detected mainly on the cut areas (*C*).

If AFM images of freeze-fractured areas of $(PC\text{-}PUs)_{2000}$ and $(PC\text{-}PU)_{1000}$ elastomers are compared, we can conclude that AFM imaging confirms the

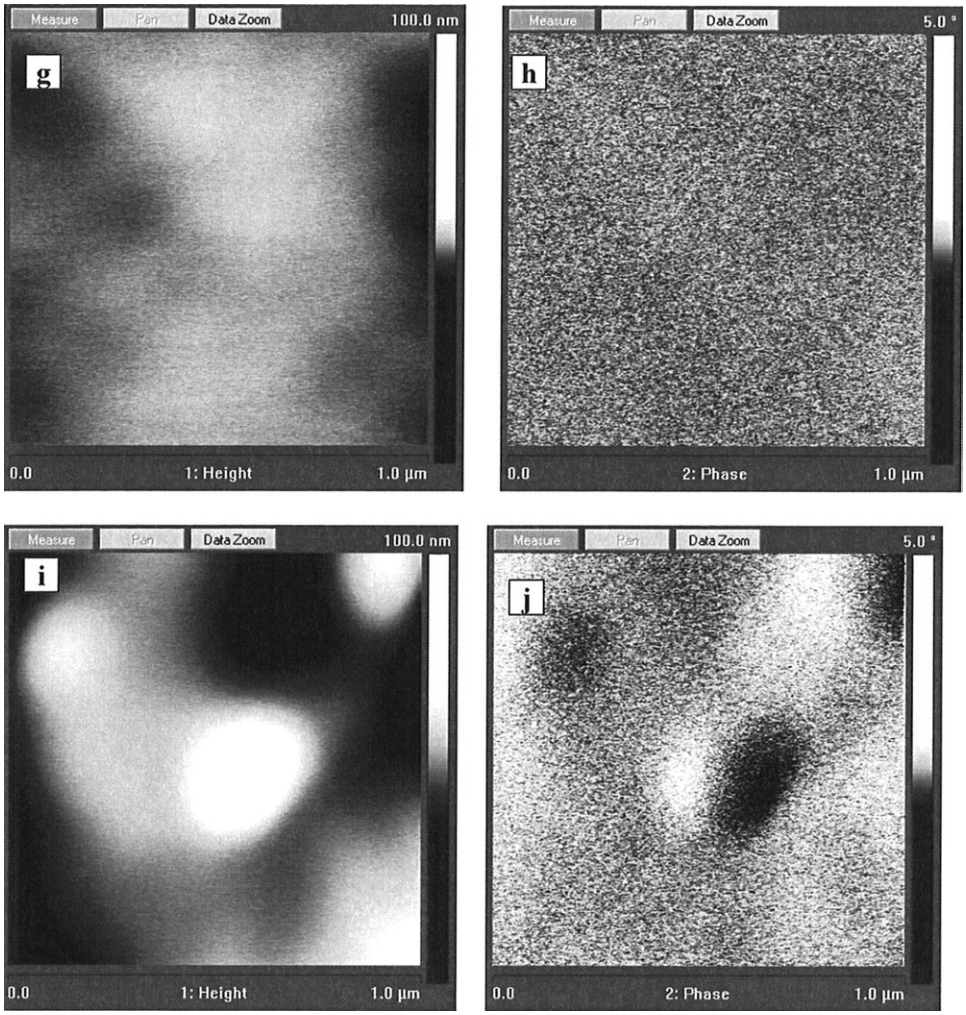

Figure 11 Continued

observations and trends already found by WAXD measurements: AFM images of PC-PUs based on both short and long MDs are very similar for given R ($R = 1$ and ∞). However, if 3D images of broken areas of samples containing similar HSC are compared, [i.e., 5652/1/0/19 Fig. 10(b), and 5651/10/0/17; Fig. 6(b)[13]] an appreciably smoother surface is observed for 5651/10/0/17. The size of spherullites detected by TEM is about 10 μm [cf. Fig. 10(h), and Fig. 5(a) in Ref. 13].

TABLE II
Characterization of Freeze-Fractured Area of Neat and Bentonite-Filled PU Sheets

Code	Surface area (μm^2)	R_q^* (nm)	R_a^{**} (nm)	R_{max}^{***} (nm)
5652/∞/0/8	100	52	43	235
5652/1/0/19	103	80	63	564
5652/1/1/19	106	121	98	833
5652/1/2/19	108	140	115	868
5652/0.3/0/35	122	354	280	2141

Surface area: the total area of examined sample surface (the three-dimensioned area of a given region expressed as the sum of the area of all the triangles formed by three adjacent data points).

R_q^* (Rms): the standard deviation of the Z values within the given area.

R_a^{**} (mean roughness): the mean value of the surface relative to the center place.

R_{max}^{***} (max height): the difference in height between the highest and lowest points on the surface relative to the mean plane

Mean: the average of all Z values within the enclosed area.

TABLE III
Characterization of Freeze-Fractured (F) and Cryo-Cut (C) Area of Neat and Bentonite-Filled PU Sheets

Code	Surface area (μm^2)	R_q^* (nm)	R_a^{**} (nm)	R_{max}^{***} (nm)
5652/∞/0/8 F	1.01	2	2	13
5652/1/0/19 F	1.03	13	10	81
5652/1/1/19 F	1.02	10	8	61
5652/1/0/19 C	1.03	3	2	15
5652/1/1/19 C	1.04	10	7	60

The explanation of values determined is the same like in Table II.

CONCLUSIONS

The formation, structure, and distribution of self-assembled of HDI/BD domains in PC-PUs and their nanocomposites spanning from the segmental level up to organized structures of micrometer size (spherullites) together with the influence of MD constitution on the efficiency of H-bond formation were studied by a combination of spectroscopy, microscopy, and scattering techniques.

Series of 5652- and 4672-based PC-PUs displayed very similar trends in spite of the differences in MD chain constitution (MD 5652 is composed from odd and even hydrocarbon units, but 4672 contains only even hydrocarbons in the polycarbonate chain). This phenomenon can be explained by the fact that less regularity of 5652 MD was balanced by higher PU chain flexibility compared with 4672 one.

Spectroscopy techniques (FTIR and solid-state NMR) confirmed high conversion of all functional groups. Careful analysis of FTIR spectra allowed discerning different types of hydrogen bonds. The intensities of "free" and H-bonded carbonyls originating from polycarbonate (soft segment) and from urethane (hard segment) in the carbonyl stretching regions from 1600 to 1800 cm^{-1} and the intensities of —NH stretching vibration bands attributed to "free" and H-bonded NH groups in the region 3200 to 3500 cm^{-1} depend strongly on the HSCs.

Very good incorporation of bentonite particles into PC-PU matrix, preferentially in HSD, was detected by techniques that probe the behavior on the sub-nanometer scale, i.e., by scattering techniques and NMR.

Fairly strong phase separation of hard and soft segments was proved by scattering methods (SAXS, WAXD). The ordering of HDI/BD building units was detected by SAXS for all samples, regardless of the fact whether they are amorphous or semicrystalline. The interdomain spacing spans from 10 to 18.7 nm, indicating strongly folded-chain conformations. In the presence of bentonite, SAXS peaks were less pronounced as compared with BO-free analogues. With increasing content of HS, a gradual change from amorphous to semicrystalline state was detected by WAXD measurements; the crystallinity transition region is about 15 wt % of HS. In accordance with NMR results, the degree of crystallinity (i.e., ordering) in BO-containing nanocomposites was the same or higher than that in BO-free analogues.

Organized structures of HS of micrometer size (spherullites) were detected by microscopy techniques (AFM and TEM). AFM images of surface topography and homogeneity do not depend only on HSCs, but they substantially differ for freeze-fractured and for cryo-cut PU sheets: While heterogeneities of nm size were clearly visible on cryo-cut samples, micrometer structures were well detected on freeze-fractured sample surfaces. Surface roughness (mostly on nm level) increase with increasing HSC and is promoted by the presence of nanofiller.

Authors thank experimental work of Mrs. Jiřina Hromádková (IMC; TEM analysis).

References

1. Hepburn, C. Polyurethane Elastomers; Elsevier, London, Great Britain, 1992. (ISBN 1–85166-589–7).
2. Prisacariu, C. Polyurethane Elastomers. From Morphology to Mechanical Aspects; Springer Verlag, Wien, Austria, 2011. (ISBN 978–3-7091–0513-9).
3. Bagdi, K.; Molnar, K.; Sajo, I.; Pukanszky, B. Express Polym Lett 2011, 5, 417.
4. Kojio, K.; Nakamura, S.; Furukawa, M. J Polym Sci Part B: Polym Phys 2008, 46, 2054.
5. Oprea, S. J Mater Sci 2011, 46, 2251.
6. Rogułska, M.; Kultys, A.; Pikus, S. J Appl Polym Sci 2008, 110, 1677.
7. Kojio, K.; Furukawa, M.; Motokucho, S.; Shimada, S.; Sakai, M. Macromolecules 2009, 42, 8322.
8. Kojio, K.; Nonaka, Y.; Masubuchi, T.; Furukawa, M. J Polym Sci Part B: Polym Phys 2004, 42, 4448.
9. Tanaka, H.; Kunimura, M. Polym Eng Sci 2002, 42, 133.
10. Hernandez, R.; Weksler, J.; Padsalgikar, A.; Choi, T.; Angelo, E.; Lin, J. S.; Xu, L. C.; Siedlecki, C. A.; Runt, J. Macromolecules 2008, 41, 9767.
11. Kultys, A.; Rogułska, M. Polym J Chem Technol 2011, 13, 23.
12. Eceiza, A.; Larranaga, M.; de la Caba, K.; Kortaberria, G.; Marieta, C.; Corcuera, M. A.; Mondragon, I. J Appl Polym Sci 2008, 108, 3092.
13. Špírková, M.; Pavličević, J.; Strachota, A.; Poręba, R.; Bera, O.; Kaprálková, L.; Baldrian, J.; Šlouf, M.; Lazić, N.; Budinski-Simendić, J. Eur Polym J 2011, 47, 959.
14. Sonnenschein, M. F.; Boyer, C.; Brune, D.; Wendt, B. L.; Myers, G.; Landes, B. Macromolecules 2011, 44, 865.

15. Mourier, E.; David, L.; Alcouffe, P.; Rochas, C.; Mechin, F.; Fulchiron, R. J Polym Sci Part B: Polym Phys 2011, 49, 801.
16. Aurilia, M.; Piscitelli, F.; Sorrentino, L.; Lavorgna, M.; Iannace, S. Eur Polym J 2011, 47, 925.
17. Bagdi, K.; Molnar, K.; Wacha, A.; Bota, A.; Pukanszky, B. Polym Int 2011, 60, 529.
18. Fernandez-d'Arlas, B.; Rueda, L.; Fernandez, R.; Khan, U.; Coleman, J. N.; Mondragon, I.; Eceiza, A. Soft Mater 2011, 9, 79.
19. Kojio, K.; Kugumiya, S.; Uchibaq, Y.; Nishino, Y.; Furukawa, M. Polym J 2009, 41, 118.
20. Ma, Z. W.; Hong, Y.; Nelson, D. M.; Pichamuthu, J. E.; Leeson, C. E.; Wagner, W. R. Biomacromolecules 2011, 12, 3265.
21. Eceiza, A.; Martin, M. D.; de la Caba, K.; Kortaberria, G.; Gabilondo, N.; Corcuera, M. A.; Mondragon, I. Polym Eng Sci 2008, 48, 297.
22. Špírková, M.; Strachota, A.; Urbanová, M.; Baldrian, J.; Brus, J.; Šlouf, M.; Kuta, A.; Hrdlička, Z. Mater Manuf Process 2009, 24, 1214.
23. Kuta, A.; Hrdlička, Z.; Strachota, A.; Špírková, M. Mater Manuf Process 2009, 24, 1185.
24. Pavličević, J.; Špírková, M.; Strachota, A.; Mészáros Szécsényi, K.; Lazić, N.; Budinski-Simendić, J. Thermochim Acta 2010, 509, 73.
25. Kultys, A.; Rogułska, M.; Pikus, S.; Skrzypiec, K. Eur Polym J 2009, 45, 2629.
26. Kultys, A.; Rogułska, M.; Gluchowska, H. Polym Int 2011, 60, 652.
27. Christenson, E. M.; Anderson, J. M.; Hiltner, A. J Biomed Mater Res A 2006, 76, 480.
28. Poręba, R.; Špírková, M.; Brožová, L.; Lazić, N.; Pavličević, J.; Strachota, A. J Appl Polym Sci, submitted
29. Li, Y.; Ren, Z.; Zhao, M.; Yang, H.; Chu, B. Macromolecules 1993, 26, 612.
30. Mishra, A.; Aswal, V. K.; Maiti, P. J Phys Chem B 2010, 114, 5292.